Solution Structure of a Complex between [*N*-MeCys^3,*N*-MeCys^7]TANDEM and [d(GATATC)]$_2$†

Kenneth J. Addess,‡ Janet S. Sinsheimer,§ and Juli Feigon*,‡

Department of Chemistry and Biochemistry and Molecular Biology Institute and Department of Biomathematics, School of Medicine, University of California, Los Angeles, California 90024

Received October 19, 1992; Revised Manuscript Received January 5, 1993

ABSTRACT: [*N*-MeCys^3,*N*-MeCys^7]TANDEM (CysMeTANDEM) is an octadepsipeptide quinoxaline antibiotic that binds specifically by bisintercalation to double-stranded DNA at NTAN sites [Addess, K. J., Gilbert, D. E., Olsen, R. K., & Feigon, J. (1992) *Biochemistry 31*, 339–350; Addess, K. J., Gilbert, D. E., & Feigon, J. (1992) in *Structure and Function Volume 1: Nucleic Acids* (Sarma, R. H., & Sarma, M. H., Eds.) pp 147–164, Adenine Press, Schenectady, NY]. We have determined the three-dimensional structure of a complex of CysMeTANDEM and the DNA hexamer [d(GATATC)]$_2$ using two-dimensional ^{1}H NMR derived NOE and dihedral bond angle constraints. This is the first structure of a TpA-specific quinoxaline antibiotic in complex with DNA. Initial structures of the complex were generated by metric matrix distance geometry followed by simulated annealing. Eight of these structures, refined by restrained molecular dynamics, energy minimization, and NOE-based relaxation matrix refinement, have an average pairwise RMSD of 1.11 Å for all structures, calculated using all heavy atoms of the drug and the DNA except the terminal base pairs. CysMeTANDEM binds to and affects the structure of the DNA in a manner similar to that observed in complexes of the CpG-specific quinoxaline antibiotics triostin A and echinomycin with DNA [Ughetto, G., Wang, A. H.-J., Quigley, G. J., van der Marel, G. A., van Boom, J. H., & Rich, A. (1985) *Nucleic Acids Res. 13*, 2305–2323; Wang, A. H.-J., Ughetto G., Quigley, G. J., Hakoshima, T., van der Marel, G. A., van Boom, J. H., & Rich, A. (1984) *Science 225*, 1115–1121; Wang, A. H.-J., Ughetto, G., Quigley, G. J., & Rich, A. (1986) *J. Biomol. Struct. Dyn. 4*, 319–342]. The two quinoxaline rings bisintercalate on either side of the two central T·A base pairs and the peptide ring lies in the minor groove. The central A·T base pairs of the complex are underwound (average helical twist angle of ~−10°) and buckle inward by ~20°. There are intermolecular hydrogen bonds between each of the Ala NH and the AN3 protons of the TpA binding site, analogous to those observed between Ala NH and GN3 in the crystal structures of the CpG-specific complexes of echinomycin and triostin A with DNA. However, the structure of the peptide ring of CysMeTANDEM in the complex differs from that of echinomycin and triostin A. This appears to be largely due to the formation of intramolecular hydrogen bonds between the two Val NH and the Ala carbonyls, which narrows the width of the peptide ring by rotating the side chains of the Val residues inward. These hydrogen bonds were also observed in the crystal structure of the related TANDEM alone [Viswamitra, M. A., Kennard, O., Cruse, W. B. T., Egert, E., Sheldrick, G. M., Jones, P. G., Waring, M. J., Wakelin, L. P. G., & Olsen, R. K. (1981) *Nature 289*, 817–819].

[*N*-MeCys^3,*N*-MeCys^7]TANDEM (hereafter referred to as CysMeTANDEM)[1] is a synthetic member of the quinoxaline family of antibiotics, which includes the naturally occurring echinomycin and triostin A. This family of drugs is characterized by a cyclic octadepsipeptide ring that is peptide bonded to two quinoxaline chromophores (Chart I). Echinomycin and triostin A are derived from *Streptomycetes* and exhibit potent antitumor activity (Katigiri et al., 1975) and contain N-methyl substituents on the Cys and Val amides. They differ from each other in the structure of the thioacetal cross-bridge. The synthetic CysMeTANDEM has the same cross-bridge as triostin A but contains an N-methyl substituent on the Cys amide only. TANDEM, another synthetic quinoxaline antibiotic, lacks N-methyl substituents on both the Cys and Val amides.

Chart I: Chemical Structure of CysMeTANDEM

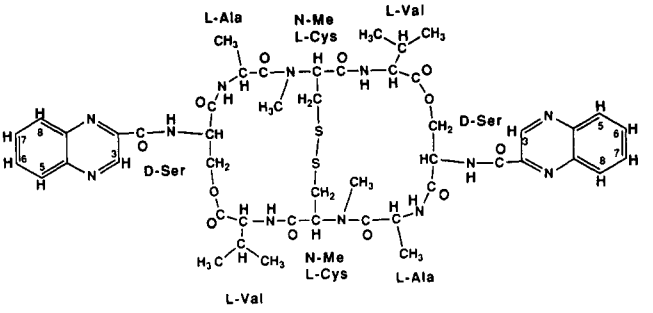

Unwinding assays and binding studies indicated that these antibiotics bind to DNA by bis-intercalation and that echinomycin and triostin A bind preferentially to G·C-rich DNA while TANDEM binds specifically to alternating A·T sequences (Lee & Waring, 1978a,b). Subsequent footprinting

† This work was supported by grants from the NIH (R01 GM 37254), by an NSF Presidential Young Investigator Award with matching funds from AmGen Inc., Monsanto Co., and Sterling Winthrop Drug Inc. to J.F., and by a USPHS national research service award (GM 08185) to J.S.S. Coordinates of all final structures have been deposited at the Protein Data Bank, Brookhaven National Laboratory, Upton, NY 11973.

‡ Department of Chemistry and Biochemistry and Molecular Biology Institute.

§ Department of Biomathematics.

[1] Abbreviations: 2D NMR, two-dimensional nuclear magnetic resonance spectroscopy; CysMeTANDEM, [*N*-MeCys^3,*N*-MeCys^7]-TANDEM; HOHAHA, homonuclear Hartmann–Hahn spectroscopy; NOESY, nuclear Overhauser effect spectroscopy; P.E.COSY, primitive exclusive COSY; P.COSY, purged COSY; RMD, restrained molecular dynamics; RMSD, root mean square difference.

0006-2960/93/0432-2498$04.00/0

studies with DNase I and MPE–Fe(II) established that echinomycin and triostin A bind specifically to sequences centered around a CpG step and that TANDEM and CysMeTANDEM bind preferentially to sequences centered around A-T-A or T-A-T (van Dyke & Dervan, 1984; Low et al., 1984a,b).

Binding of echinomycin and triostin A to DNA has been studied extensively both by crystallography (Ughetto, 1985; Wang et al., 1984, 1986) and by NMR (Gao & Patel, 1988; Gilbert et al., 1989; Gilbert & Feigon, 1989, 1992). These studies showed directly that echinomycin and triostin A bind specifically in the minor groove of the DNA at NCGN sites by bis-intercalation with their quinoxaline rings bracketing the CpG step. Intercalation by each drug causes the DNA to unwind by ~26° at the CpG step and causes the base pairs of the CpG step to buckle inward by about 20° (Ughetto et al., 1985; Wang et al., 1984, 1986). On the basis of the crystal structures of 2:1 drug–DNA complexes, Rich and co-workers proposed that the structural basis of the sequence specific binding of triostin A and echinomycin to NCGN sites was the formation of two intermolecular hydrogen bonds, one between the Ala NH of the drug and GN3 and the other between the Ala CO and GN2 (Ughetto et al., 1985; Wang et al., 1984, 1986). An additional feature in the crystal structures of the 2:1 drug–DNA complexes was Hoogsteen hydrogen bonding in the A·T base pairs on either side of the CpG binding site. However, solution NMR studies of related complexes showed that Hoogsteen base pair formation in these complexes was both sequence and temperature dependent (Gao & Patel, 1988; Gilbert et al., 1989; Gilbert & Feigon, 1989, 1992).

Interactions between the A·T-specific TANDEM and CysMeTANDEM and DNA have been much less studied. Both TANDEM and CysMeTANDEM bind more weakly to DNA than echinomycin and triostin A. Footprinting studies by Waring and co-workers showed that CysMeTANDEM did not inhibit the activity of the restriction enzyme *Sau*3AI, which restricts GATC site, but did inhibit the activity of the enzyme *Rsa*I, which restricts GTAC. This led them to propose that CysMeTANDEM prefers TpA to ApT steps. However, they could not firmly establish the sequence specificity of CysMeTANDEM because echinomycin was unexpectedly shown to inhibit both restriction enzymes (Low et al., 1986). NMR studies by Powers et al. (1989) of the binding of CysMeTANDEM to the decamer $[d(CCCGATCGGG)]_2$ indicated that CysMeTANDEM did not bind to this DNA by intercalation, and they concluded that CysMeTANDEM binds to this sequence in the minor groove.

We recently reported NMR studies on the binding of CysMeTANDEM to the DNA octamers $[d(GGATATCC)]_2$ and $[d(GGTTAACC)]_2$. The results of these studies show unambiguously that CysMeTANDEM binds specifically to a TpA step, and not to an ApT step, by bis-intercalation (Addess et al., 1992a,b). More recent footprinting studies by Fox and co-workers also indicate that CysMeTANDEM binds selectively at TpA steps (Waterloh et al., 1992).

Here we present the three-dimensional solution structure of a CysMeTANDEM–$[d(GATATC)]_2$ complex. The structure of the DNA hexamer rather than one of the octamer complexes was solved because most of the cross peaks in the two-dimensional NOESY (Kumar et al., 1980) spectra of the hexamer complex are resolved, thus allowing for accurate integration of cross peaks for the structure determination. This is the first three-dimensional structure of a TpA-specific quinoxaline antibiotic–DNA complex. No starting model was used in the structure determination, and the drug was not docked onto the DNA. Instead, initial structures of the CysMeTANDEM–$[d(GATATC)]_2$ complex were generated by metric matrix distance geometry. These structures were refined by energy minimization, restrained molecular dynamics, and direct NOE refinement. Eight refined structures have an average pairwise RMSD for all heavy atoms except the terminal base pairs of 1.1 Å. Details of the structure are presented and compared with the crystal structures of triostin A–DNA complexes.

MATERIALS AND METHODS

Sample Preparation. The hexamer $d(G_1A_2T_3A_4T_5C_6)$ was synthesized on an ABI 381A synthesizer using β-cyanothethyl phosphoramidite chemistry on a 10-μmol scale and purified by gel filtration as previously described. NMR samples of the free DNA and the DNA–drug complex were prepared as previously described (Addess et al., 1992a). Samples contained ~2 mM DNA duplex, 200 mM NaCl, and 5 mM $MgCl_2$, pH 6.6, with or without added drug. CysMeTANDEM was a gift from Richard Olsen.

NMR Spectroscopy. All NMR experiments were done at 500 MHz on a General Electric GN500 spectrometer. Phase-sensitive nuclear Overhauser effect (NOESY) spectra in D_2O were acquired using the method of States et al. (1982) with preirradiation of the HDO peak during the recycle delay (Kumar et al., 1980). NOESY spectra used in the structure determination were obtained at six different mixing times of 25, 50, 75, 100, 125, and 150 ms over a 6 day period without removing the sample from the magnet. Phase-sensitive NOESY spectra in H_2O were obtained by replacing the last 90° pulse with a $1\bar{1}$ spin echo pulse sequence and the appropriate phase cycle to suppress the large water resonance (Sklenář & Bax, 1987). The carrier was centered at the water resonance, and the delay τ was adjusted so that the excitation mixture was at ~12 ppm. HOHAHA spectra were acquired using the MLEV17 mixing sequence and 1.5-ms trim pulses for the spin lock (Bax & Davis, 1985). P.COSY spectra were acquired with a flip angle mixing pulse of 90° (Marion & Bax, 1988). P.E.COSY spectra were acquired with a mixing pulse of 35° (Mueller, 1987). All 2D NMR spectra were processed on a Personal Iris 4D25 using the Fortran program FTNMR (Hare Research). NOESY spectra were baseline flattened with a first-order polynomial in t_2 and with a second-order polynomial in t_1. T_1 ridge noise was minimized by multiplying the first row by $^1/_2$ (Otting et al., 1986). Detailed descriptions of other acquisition and processing parameters are given in the figure captions.

Determination of Distances and Distance Geometry. NOE cross peak volumes of the nonexchangeable proton resonances at the six different mixing times were obtained by cross peak integration using the FTNMR software. NOE cross peak volumes of exchangeable proton resonances were obtained by cross peak integration of a NOESY spectrum of the sample in H_2O acquired with $\tau_m = 70$ ms and a $1\bar{1}$ echo observe pulse. Calculating the volumes involves summing all the points of the transformed spectra within the limits of an ellipse that surrounds the cross peak. Initial buildup rates were obtained from the cross peak intensities in the NOESY spectra at the six different mixing times by stepwise regression using the BMDP statistical package (BMDP Statistical Software Inc., 1990). These rates were converted into distances by the two-spin approximation, using the CH5–CH6 distance of 2.44 as a calibration. The distances obtained for cross peaks on both side of the diagonal were averaged. The lower bounds for distances between nonexchangeable protons were set to 1.9

Å, while the upper bounds that were used depended on the distance between the two protons, as follows: $d \leq 3.0$, upper bound $1.1d$; $3.0 < d \leq 3.5$, upper bound $1.2d$; $3.5 < d \leq 4.5$, upper bound $1.3d$; and $4.5 < d$, upper bound $1.4d$. For distances involving exchangeable resonances, the upper bound was increased by 20% to account for a possible decrease in the NOE cross peak volume due to exchange with H_2O. A total of 548 distance constraints, i.e., 2×274 asymmetric distance constraints, were used to generate starting structures. Of the 274 asymmetric distance constraints, 62 were constraints between the drug and the DNA. Although the complex is 2-fold symmetric in solution, no symmetry constraints were imposed during the refinement.

Twenty starting structures were generated by embedding distances into Cartesian space using the distance geometry algorithm (Crippen & Havel, 1988). Of these, the 10 with lowest energies were used in the subsequent refinement. Two of the structures (F_1 and F_2) were generated by full embedding procedure using the computer program DSPACE (Hare Research), while the remainder (S3-S10) were generated with the substructure embedding routine in XPLOR (Kuszewski et al., 1992). In the substructure embedding routine, 184 of the 512 atoms of CysMeTANDEM were embedded into Cartesian space. The 10 embedded structures were refined by using the standard energy minimization and simulated annealing routines in either DSPACE or XPLOR. All refined starting structures contained no distance violations greater than 0.2 Å.

Determination of Dihedral Bond Angles. The $J_{1'2'}$, $J_{1'2''}$, $J_{2'3'}$, $J_{2''3'}$, and $J_{3'4'}$ values were obtained by simulation of H1′–H2′,H2″ and H2′,H2″–H3′ cross peak patterns in a P.COSY spectrum using the SPHINX/LINSHA software (Widmer & Wüthrich, 1987) as previously described (Addess et al., 1992a). These coupling constants were used to derive the torsional angles by solving the modified Karplus equation (Haasnoot et al., 1980).

All of the ϵ torsion angles (C4′–C3′–O–P) of the phosphodiester backbone could be qualitatively constrained to the ranges 130°–200° (BI phosphate conformation) and 250°–320° (BII phosphate conformation) on the basis of the values for $\sum J_{H3'}$, which is the summation of the $J_{2'3'}$ $J_{2''3'}$, $J_{3'4'}$, and $J_{P3'}$, measured from a P.E.COSY spectrum (Kim et al., 1992). Values of 15–18 Hz for $\sum J_{H3'}$ were obtained for all DNA residues except T3, which had a value of 28.9 Hz. According to a contour map of $\sum J_{H3'}$ as a function ϵ and P phase angle of the sugar [Figure 6 of Kim et al. (1992)], all values of $\sum J_{H3'}$ fall within the ranges for ϵ values of BI or BII phosphate type at the appropriate P value for each sugar.

All torsional angle restraints discussed above were introduced into the minimization, dynamics, and relaxation refinement stages of the structure calculations.

Restrained Molecular Dynamics. The restrained molecular dynamics (RMD) and Powell minimizations were done with XPLOR (Brünger, 1990), using the Charmm force field. Hydrogen bonds were not included as an explicit potential energy term. Instead, hydrogen bonds were included as distance restraints. Each starting structure was subjected to 10 000 cycles of energy minimization to relieve bond length and angle violations from the starting structure. During the minimization, the potential energy terms for the NOE distance and the dihedral angle restraints were included in the total energy function. The resulting structures were then subjected to restrained molecular dynamics. A total of 20 ps of Verlet dynamics was performed in three stages. In the first stage, each molecule underwent heating from 300 to 1000 K in 35 cycles. During that time, the energy terms for the NOE distance restraint and the dihedral angle restraint were turned off. In the first cycle, Newton's equations of motion were integrated with initial velocities taken from a Maxwellian distribution at 300 K in 100 steps with a time step of 0.001 ps. During the second stage, the scale factor of the NOE force constant was increased to 10 and the scale factor of the dihedral force constant was increased to 1 in 10 cycles. For each cycle, Newton's equations were integrated with initial velocities taken from a Maxwellian distribution at 1000 K, in 1000 steps with a time step of 0.001 ps. During the last cycle, each structure was cooled slowly to 300 K with the NOE and dihedral bond angle scale factors remaining constant. Finally, each structure was subject to from 10 000–20 000 cycles of minimization until the energy gradient converged.

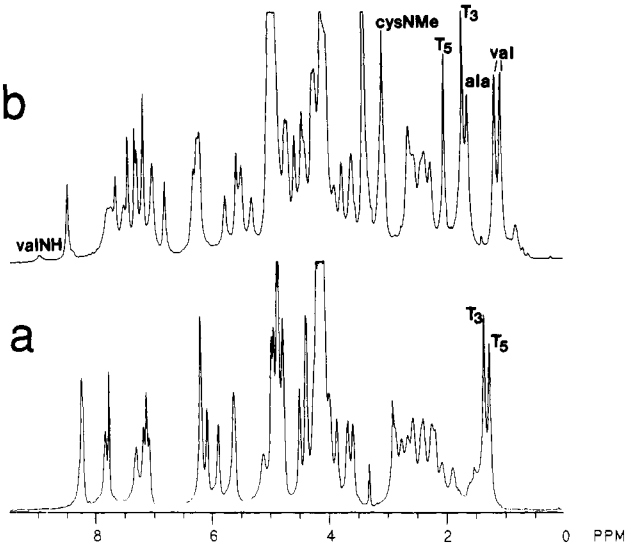

FIGURE 1: One-dimensional ^{1}H NMR spectra of (a) $[d(GATATC)]_2$ and (b) the 1:1 complex of CysMeTANDEM + $[d(GATATC)]_2$ in D_2O at 15 °C. Sample are 2 mM DNA duplex, 200 mM NaCl, and 5 mM $MgCl_2$, pH 6.5. Assignments of the thymine methyls, the Ala methyl, the Val methyl, and the Val NH are indicated. The spectra were acquired with a sweep width of 5000 Hz in 2K complex points and line broadened by 3 Hz prior to Fourier transformations.

Volume-Based Relaxation Matrix Refinement. In a last step of refinement, direct NOE refinement (Yip & Case, 1989) of the structures was done using the relax option in XPLOR (Nilges et al., 1991). The relax option of XPLOR fits the coordinates to the experimental volumes directly, rather than fitting them to distance bounds. The theoretical volumes are calculated from a total relaxation of a coordinate set that is either minimized by Powell or subjected to RMD (Nilges et al., 1991). The R factor, $R(F) = \sum(|vol_{cal} - vol_{exp}|)/\sum|vol_{exp}|$, where vol_{cal} is the volume calculated from the total relaxation matrix and vol_{exp} is the experimental volume (Gonzalez et al., 1991), was used to compare the final results to the experimental volumes. Of the 10 refined structures, one had a significantly higher R factor than the others (0.26) and one had significantly higher pairwise RMSDs (1.3). The eight remaining structures are given under Results.

Calculation of Structural Parameters. Helical twist angles, buckling of the bases, and sugar geometries of the structures were calculated with the program NEWHELIX91 (obtained from R. E. Dickerson).

RESULTS

CysMeTANDEM Complex Formation. One-dimensional ^{1}H NMR spectra of $[d(GATATC)]_2$ containing no drug and

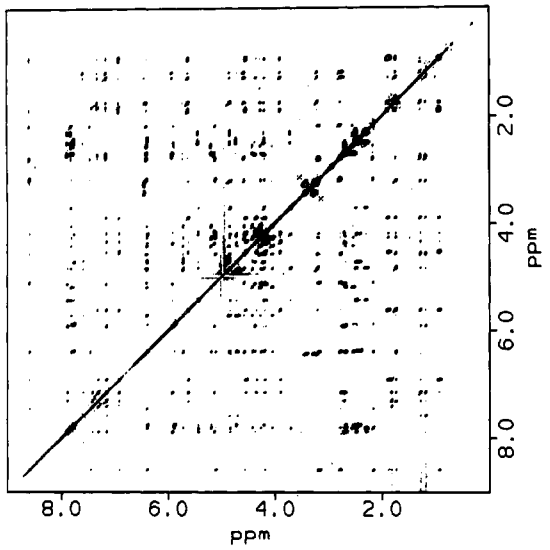

FIGURE 2: NOESY spectrum of the 1:1 CysMeTANDEM–[d(GATATC)]$_2$ complex in D_2O at 25 °C with τ_m = 150 ms. Sample conditions were the same as Figure 1b. The spectrum was acquired with a sweep width of 5000 Hz in both dimensions, 291 t_1 values of 64 scans, and 2K complex points. A total of 291 points were apodized in both dimensions with sine-bell phase shifted by 90°. Data in t_1 were zero filled to 1K prior to Fourier transformation.

one drug per duplex in D_2O are shown in Figure 1. The spectral changes that occur upon addition of the drug to the DNA hexamer are the similar to those observed upon complex formation of CysMeTANDEM with the octamers [d(GGATATCC)]$_2$ and [d(GGTTAACC)]$_2$ (Addess et al., 1992a). Complex formation is illustrated by the change in the chemical shifts of the two thymine methyls and the appearance of the Ala methyl, Val methyls and CysNMe resonances, which are labeled. As in the case of the two octamer complexes, no doubling of the DNA and drug resonances are observed for the fully saturated complex, which indicates that both the DNA and the drug retain their 2-fold symmetry on complex formation.

Assignment of the Resonances in the CysMeTANDEM–[d(GATATC)]$_2$ Complex. Assignments of the proton resonances of the DNA and CysMeTANDEM in the 1:1 complex were obtained by analysis of NOESY, P.COSY, and HOHAHA spectra essentially as described for the complexes of CysMeTANDEM with the DNA octamers [d(GGATATCC)]$_2$ and [d(GGTTAACC)]$_2$ (Addess et al., 1992a). A NOESY spectrum of the 1:1 CysMeTANDEM–[d(GATATC)]$_2$ complex is shown in Figure 2. The resolution of this spectrum was good enough to allow assignment of all the proton resonances of the DNA and the drug except a couple H5′,H5″ (Table I). Furthermore, almost all of the cross peaks could be integrated, which was essential for calculating a well-defined structure of the complex.

The cross peak patterns for [d(GATATC)]$_2$ and CysMeTANDEM in the complex were similar to those observed for the complexes of CysMeTANDEM with the octamers [d(GGATATCC)]$_2$ and [d(GGTTAACC)]$_2$ (Addess et al., 1992a). Both the H2′ and H2″ resonances of the T and A in the TpA step have unusual chemical shifts; T_3H2′ and T_3H2″ are upfield shifted by ~1 ppm relative to the free DNA and A_4H2′ resonances downfield of A_4H2″ rather than upfield as in the free DNA. The T_3 imino is shifted upfield ~2 ppm relative to the T_3 imino of the free DNA, indicative of intercalative binding near the central A·T base pairs (Feigon et al., 1984).

Stereospecific assignments of the Val methyls were obtained on the basis of a strong NOE between the Val βH and Ser NH resonances. In the model of the drug, the distance between the Val βH and the Ser NH is ~2.5 Å when the dihedral between the Val αH and the Val βH is 180° while it is ~4.5 Å when the dihedral between the Val αH and the Val βH is 0°. This enabled us to determine the proper orientation of the Val methyls with respect to the Val NH and other protons that displayed different NOE intensities to each Val methyl.

Structure Generation and Initial Refinement. The intensity of the single CH5–CH6 cross peak was used as the internal standard for interproton distances. In order to check the accuracy of the distance calibration, the interproton distances obtained for the two best resolved of the six H2′–H2″ cross peaks were compared to the known H2′–H2″ distance of 1.77 Å. The calculated H2′–H2″ distances were 1.8 ± 0.2 Å for A_4 and 1.9 ± 0.2 Å for T_3. This indicates that the starting distances are reasonably accurate and is consistent with the results of Reid and co-workers (Nerdal et al, 1988), who found that the correlation times for the base CH5–CH6 vectors and sugar H2′–H2″ vectors were not significantly different from each other.

One of the starting structures (after embedding and before RMD) is shown in Figure 3. Although several NMR structures of drug–DNA complexes have been published, these structures are usually generated by refinement of an initial starting model for the DNA onto which the drug is docked.

Table I: Assignments of the [*N*-MeCys]^3,[*N*-MeCys]^{7}TANDEM–[d(GATATC)]$_2$ Complex

	[d(GATATC)]$_2$ Chemical Shifts (ppm)[a]									
	H8/H6	Me/H5 H2	H1′	H2′	H2″	H3′	H4′	H5′,H5″	imino[b]	amino[b]
G_1	7.60		5.20	2.06	2.25	4.62	3.49		12.78	
A_2	7.67	7.36	5.69	2.48	2.48	4.90	4.61	4.26, 4.38		6.76
T_3	6.70	1.60	5.39	0.69	1.65	4.32	3.67	4.38, 4.24	11.53	
A_4	8.37	7.09	6.16	2.94	2.55	4.89	4.36	4.23, 4.37		
T_5	7.58	1.93	6.17	2.31	2.45	4.97	3.82	4.07, 4.30	13.06	
C_6	7.54	5.65	6.15	2.17	2.22	4.50	3.97			6.61, 7.24

	[*N*-MeCys^3,*N*-MeCys^7]TANDEM Chemical Shifts (ppm)[a]						
	α	β	β′	γ	γ′	NH	NMe
serine	5.50	4.47	4.62			8.51	
valine	4.39	2.55		0.94	1.06	8.91	
cysteine	6.21	3.04	3.18				2.98
alanine	4.62	1.51				9.76	
	3	5	6	7	8		
quinoxaline	7.23	7.20	7.09	6.92	6.93		

[a] Chemical shifts relative to DSS. [b] Chemical shifts at 10 °C.

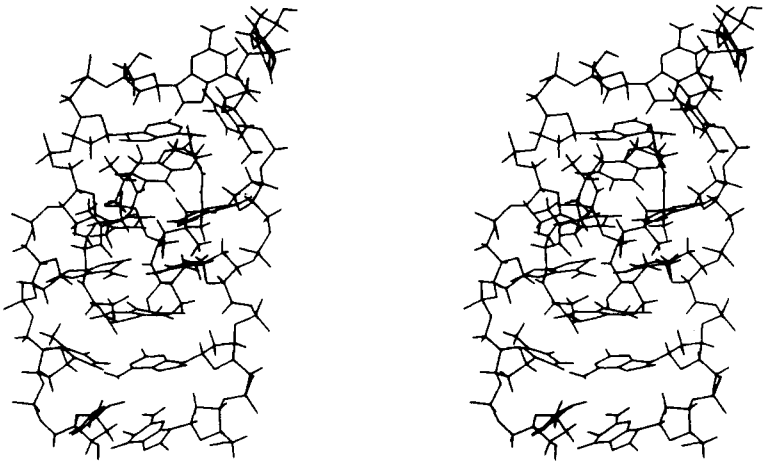

FIGURE 3: Stereoview of F_1, one of the 10 starting structures of CysMeTANDEM–[d(GATATC)]$_2$. The structure was generated by distance geometry using the full embedding procedure in the program DSPACE, as described under Materials and Methods.

Table II

Atomic RMS Differences (Å) between Structures Obtained by Relaxation Matrix Refinement of CysMeTANDEM–[d(GATATC)]$_2$

structure	F_1	F_2	S_4	S_5	S_6	S_7	S_8	S_{10}
F_1		0.85	1.11	0.96	0.92	1.20	1.08	1.25
F_2			0.87	0.78	0.88	1.04	1.04	1.23
S_4				0.80	1.04	0.91	1.18	1.04
S_5					0.82	0.95	1.08	1.15
S_6						1.01	1.12	1.19
S_7							1.27	1.00
S_8								1.40
S_{10}								

Atomic RMS Differences (Å) between Starting Structures CysMeTANDEM–[d(GATATC)]$_2$

structure	F_1	F_2	S_3	S_4	S_5	S_6	S_7	S_8	S_9	S_{10}
F_1		1.75	2.27	2.17	2.08	2.96	3.47	2.95	3.40	3.08
F_2			1.97	2.10	1.91	2.70	3.42	2.84	3.14	2.97
S_3				1.82	1.83	1.74	2.28	1.84	2.24	1.99
S_4					1.64	2.35	3.00	2.48	2.99	2.56
S_5						2.62	3.03	2.49	3.21	2.75
S_6							2.00	1.69	1.41	1.39
S_7								1.26	1.87	1.81
S_8									1.72	1.57
S_9										1.58
S_{10}										

This work represents to our knowledge the first solution structure of a drug–DNA complex that was solved by refinement of initial structures generated by metric matrix distance geometry for the entire complex. Thus it was of interest to see how well the initial embedding works. The starting structure shows that the embedding procedure generates a structure that reflects many of the qualitative observations of the NMR studies (Addess et al., 1992a). All of the starting structures have a right-handed DNA helix with the CysMeTANDEM binding by bis-intercalation with the quinoxaline rings bracketing the TpA steps and the peptide ring in the minor groove. The average pairwise RMSDs for heavy atoms of all 10 starting structures was 2.28 ± 0.32 Å excluding the terminal base pairs and 3.02 ± 0.85 Å if the less well constrained terminal base pairs are included. Pairwise RMSDs between structures are given in Table II.

Although the initial embed generated reasonable starting structures, all of the starting structures contained several covalent bond and dihedral bond angle violations. In particular, the bases and the quinoxaline rings were distorted and nonplanar. To relieve these distortions, 10 000 cycles of energy minimization were run, followed by 20 ps of restrained molecular dynamics and by enough cycles of minimization to cause the gradient of all structures to converge. Originally, the DNA bases contained improper force constants that were not strong enough to flatten the bases during the refinement process. To correct this problem, the force constant for all the impropers was increased 10-fold to the same value used for all the impropers in the quinoxaline rings. This stage of refinement resulted in a significant improvement of the total energy, with the most significant improvement occurring in the covalent bond, dihedral angle, and improper energy terms.

Relaxation Matrix Refinement. Further refinement of the structures was done by replacing the distance constraints with NOE volume constraints, which caused a significant improvement in the *R* factor. However, the movement of the atoms during this stage of refinement was minimal. This indicates that the *R* factor is very sensitive to small changes in the atomic positions of the complex (Nilges et al., 1991). This also indicates that the positions of the atoms of the MD refined structures are more or less accurately defined by the set of distance restraints used in the distance geometry and molecular dynamics stages of the structure determination. The average pairwise RMSD calculated for all atoms between each of the eight final relaxation matrix refined structures and the MD refined structures is 0.72 ± 0.07 Å. The pairwise RMSDs for the eight final refined structures are given in Table II.

The most well-defined portions of the structures are the backbone conformation of the drug and the four internal base pairs, while the greatest variation among the 10 structures is in the phosphate backbone (Figure 4). The variation in the phosphate backbone is caused principally by lack of experimental constraints, though the motion of the phosphate backbone may also contribute to this variation. The average pairwise RMSD for the drug alone is 1.01 ± 0.12 Å. When the Val side chains are deleted from this analysis, the RMSD decreases to 0.63 ± 0.24 Å, which indicates that the conformation of the backbone atoms of the octadepsipeptide ring and the position of the quinoxaline rings within the two sites of intercalation are well defined. The average pairwise RMSD for the base pairs and deoxyribose sugars of the four internal residues is 0.75 ± 0.21 Å, while the average pairwise RMSD of the phosphate backbone for these four residues is 1.44 ± 0.24 Å. The average *R* factors for the eight structures were 0.48 ± 0.09 (starting), 0.54 ± 0.03 (RMD), and 0.21 ± 0.01 (final).

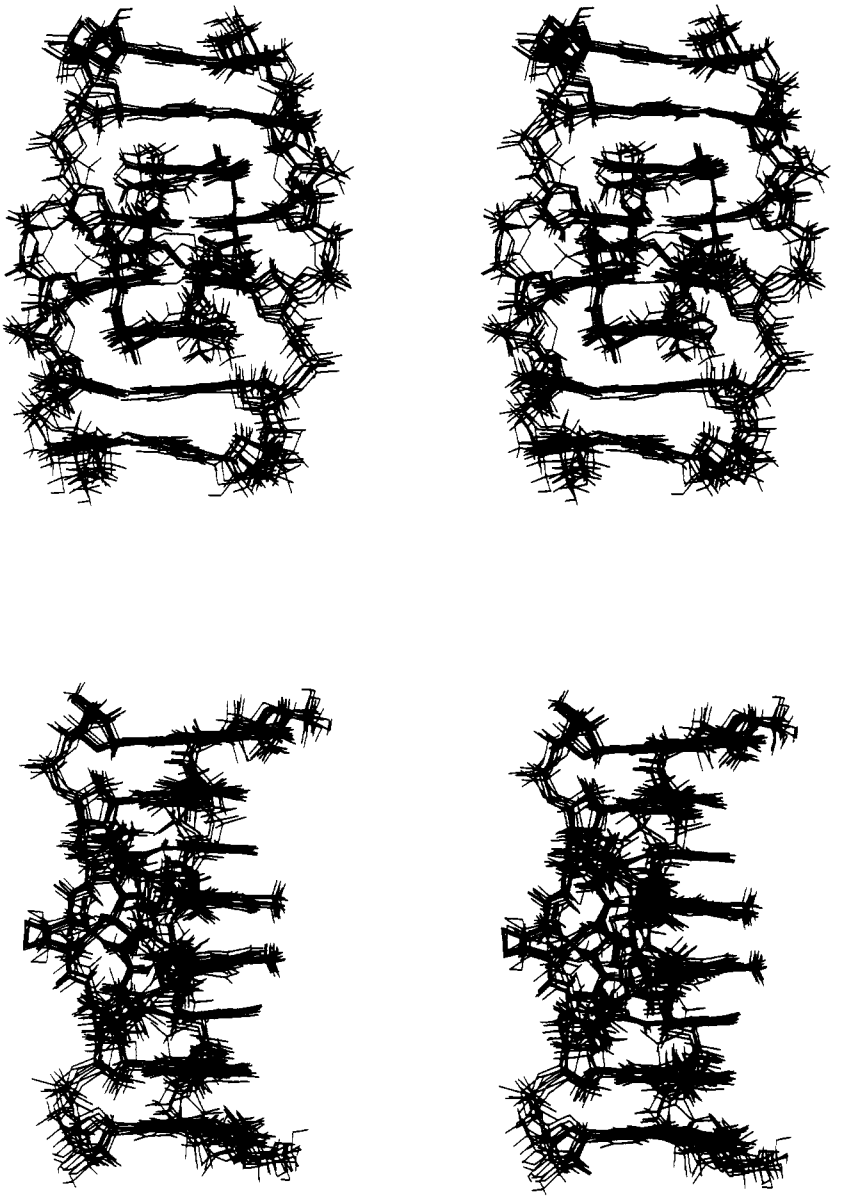

FIGURE 4: Stereoviews of (a, top) the front and (b, bottom) the side of the 10 superimposed final structures of CysMeTANDEM–[d(GATATC)]$_2$. These final structures were obtained by molecular dynamics, minimization, and relaxation matrix refinement, using the program XPLOR.

DISCUSSION

Three-Dimensional Structure of the CysMeTANDEM–[d(GATATC)]$_2$ Complex. Stereoviews of the eight final refined structures are shown superimposed in Figure 4. The complex is 2-fold symmetric, with the 2-fold axis of symmetry located between the symmetry-related T_3·A_4 base pairs. Since symmetry was not imposed during the refinement, the variations in the two strands and the two symmetrical halves of the CysMeTANDEM represent essentially a doubling of the number of structures shown. The minor groove view (Figure 4a) shows the peptide ring bound in the minor groove, with the two quinoxaline rings intercalated on either side of the central T_3·A_4 base pairs. The DNA helix unwinds significantly (discussed below) and the distance between base pairs A_2·T_5 and T_3·A_4 increases from an average of ~3.5 to ~5.0 Å to allow intercalation of the quinoxaline rings.

A space-filling model of the structure of the CysMeTANDEM–[d(GATATC)]$_2$ complex is shown in Figure 5. The major groove view (Figure 5a) shows the edge of the two quinoxaline rings intercalated on either side of the central T_3·A_4 base pairs. The peptide ring fills the minor groove (Figure 5b). There are several van der Waals interactions between the sugar protons in the $A_2T_3A_4T_5$ binding site and the Ala and Val side chains of the octadepsipeptide ring as well as specific hydrogen bonds between the Ala NH and the A_4N3 (discussed below).

Unwinding of the DNA in the Complex. A stereoview of the structure of the DNA in the complex without the drug is shown in Figure 6. The principle changes in the DNA conformation caused by intercalation, besides separation of the A_2·T_5 and T_3·A_4 base pairs to accommodate the quinoxaline rings, are unwinding of the helix and buckling of the base pairs flanking the site of intercalation. These conformational changes appear to be a direct effect of stacking of the bases with the quinoxaline rings (Figure 7).

Figure 8 shows the helical twist angle as a function of base residue. The most significant unwinding of the DNA in the complex occurs at the TpA step, which is adjacent to the site of intercalation. The average helical twist angle between the A·T base pairs of the TpA step is $-10.8 \pm 2.6°$. The average helical twist angle between the base pairs in either side of the quinoxaline ring is $-25.1 \pm 2.5°$. The uncertainty in the helical

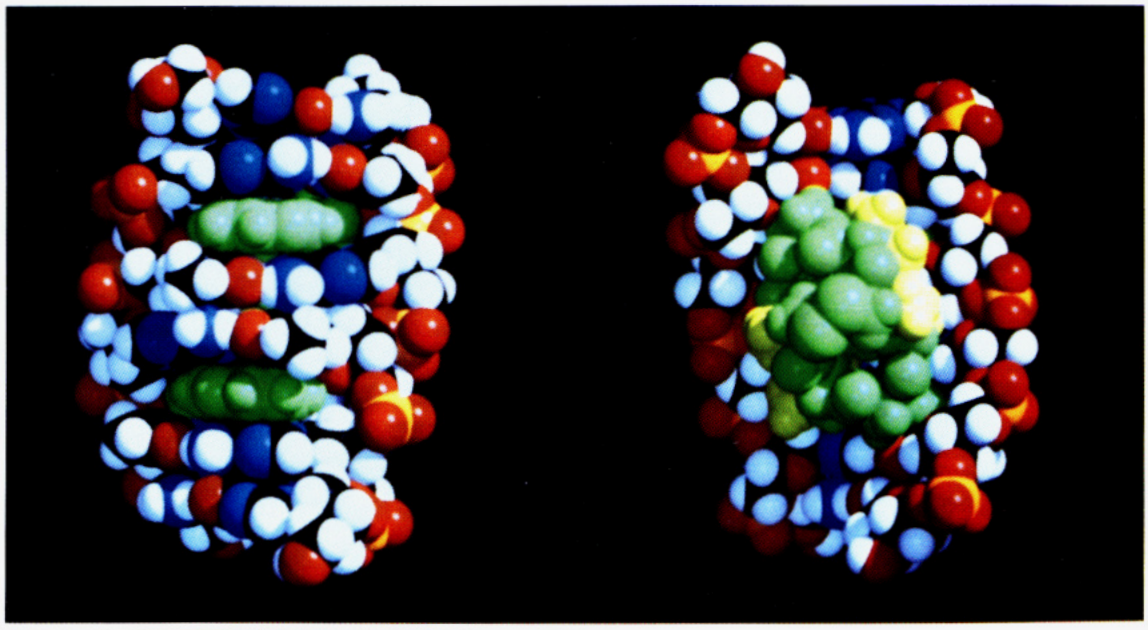

FIGURE 5: Space-filling view of the structure of CysMeTANDEM–[d(GATATC)]$_2$. (a) View from the major groove; (b) view from the minor groove. The CysMeTANDEM is colored in green; the valine methyls and alanine methyls on CysMeTANDEM are yellow.

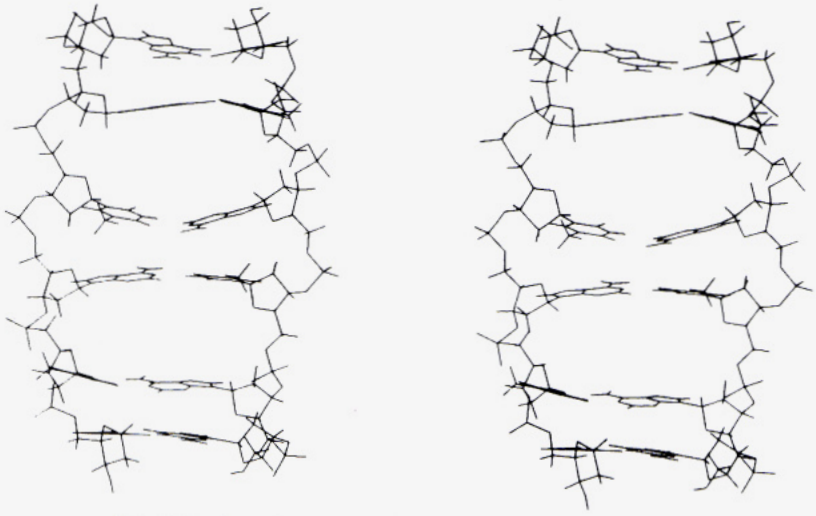

FIGURE 6: Stereoview of the structure of the DNA from the complex of CysMeTANDEM–[d(GATATC)]$_2$. The view is from the major groove side.

twist angle of each of the various structures can largely be attributed to lack of constraints in the phosphate backbone, which has an average pairwise RMSD that was much higher than the average pairwise RMSD for the rest of the molecule.

The unwinding pattern of the DNA in the CysMeTANDEM–[d(GATATC)]$_2$ complex is characteristic of perpendicular intercalators, which contain bulky substituents such as a peptide ring along the long axis of their intercalative moieties and intercalates DNA with their long axes nearly perpendicular to the long axes of the DNA bases. Crystal structures of other perpendicular intercalators such as triostin A, daunomycin, and the crystal and solution structures of nogalamycin complexed to DNA show that each of these drugs, like CysMeTANDEM, unwinds the DNA significantly at the step adjacent to the site of intercalation and not at the site of intercalation itself (Egli et al., 1991; Gao et al., 1990; Nunn et al., 1991; Ughetto et al., 1985; Wang et al., 1984, 1986; Zhang & Patel, 1990). In the crystal structures of triostin A–DNA complexes, the helical twist angle of the DNA at the CpG steps is ~−10° (Wang et al., 1984; Ughetto et al., 1985).

Stacking Interactions. Figure 7 illustrates the stacking of the bases and the quinoxaline viewed down the helical axis. The quinoxaline ring stacks over the A_2 base in the A_2·T_5 base pair, while it has little or no overlap with the T_5 base. Both the T_3 and A_4 bases of the T_3·A_4 base pair overlap only partially with the quinoxaline base. At the central T_3pA_4 step, there are strong stacking interaction between the T_3 and A_4 of adjacent T_3·A_4 base pairs. This pattern of stacking interactions is similar to the stacking that is observed between the quinoxaline of triostin A and the C·G base pairs of the CpG binding site (Wang et al., 1984; Ughetto et al., 1985). Williams et al. (1992) argue that the observed unwinding pattern is caused by the long axis of the intercalator orienting itself nearly perpendicular to the long axis of the DNA base pairs flanking the intercalation site. For this reason, significant unwinding of the bases at the site of intercalation contributes little or no increase in the stacking interactions, while unwinding of the base pairs between the sites of intercalation contributes to a large increase in the stacking interactions.

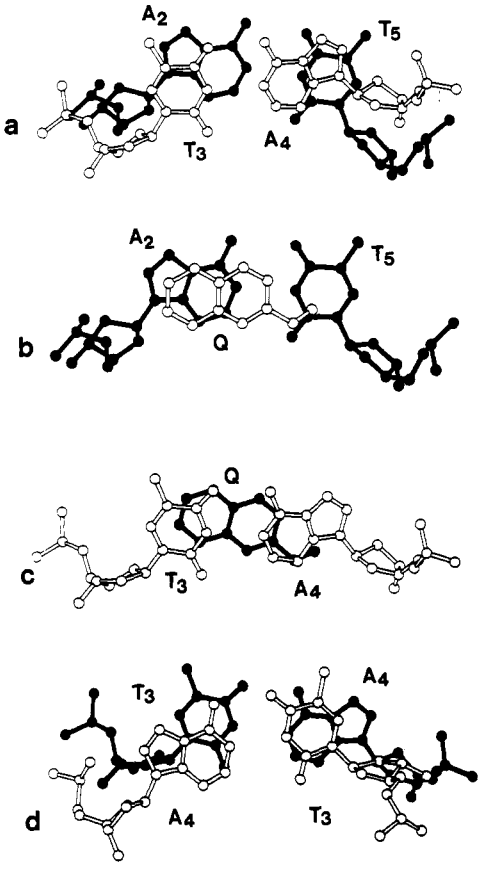

FIGURE 7: Stacking arrangements of the bases and the quinoxaline rings as viewed down the helical axis. Shown are stacking between (a) A_2·T_5 and T_3·A_4 (with the quinoxaline ring deleted), (b) A_2·T_5 and quinoxaline ring, (c) quinoxaline ring and T_3·A_4, and (d) the two T_3·A_4 base pairs.

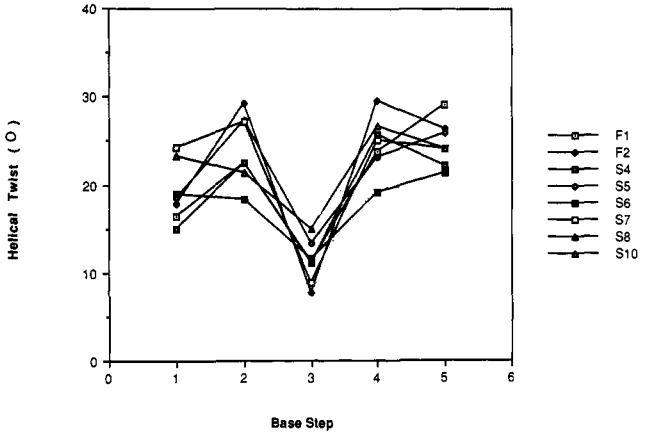

FIGURE 8: Plot of global helical twist angle as a function of base step for the eight final structures of CysMeTANDEM–[d(GATATC)]$_2$.

Figure 7 also shows that A_2·T_5 forms a Watson–Crick base pair. In the crystal structure of the 2:1 triostin A–[d(CGTACG)]$_2$ complex, the A·T base pairs flanking the two CpG binding sites are Hoogsteen base paired with the A in the syn conformation (Wang et al., 1984; Ughetto et al., 1985). The authors argue that this increases the stacking interactions. However, solution studies of the 2:1 echinomycin–[d(ACGTACGT)]$_2$ (Gilbert & Feigon, 1991) as well as 2:1 CysMeTANDEM–[d(ATACGTAT)]$_2$ complexes (Addess et al., 1992b) indicated that only the terminal A·T base pairs formed stable Hoogsteen base pairs at room temperture. In addition, no Hoogsteen base pairs have been observed in any of the solution complexes of echinomycin or CysMeTANDEM when there is only a single binding site flanked by two or more base pairs (Gilbert & Feigon, 1992; Gao & Patel, 1988, 1989; Addess et al., 1992a,b).

Table III: Sugar Conformations of CysMeTANDEM–[d(GATATC)]$_2$

	pseudorotation phase angle P (deg)	puckering amplitude τ_m (deg)	puckering mode
G_1	183.5 ± 4	46.4 ± 2	C3′ exo
A_2	118.8 ± 27	39.9 ± 6	C1′ exo
T_3	59.3 ● 6	39.0 ± 3	C4′ exo
A_4	135.3 ± 16	40.8 ± 4	C1′ exo
T_5	103.5 ± 13	37.6 ± 8	C1′ exo
C_6	25.8 ± 2	45.9 ● 2	C3′ endo

Buckling of the A·T Base Pairs in the Complex at the Binding Site. For each structure, significant buckling occurs in the base pairs flanking the intercalation sites (Figure 6). The inward buckle of the T_3·A_4 base pair averages 18.2 ± 3.6°, and the outward buckle of the A_2·T_5 base pair averages 14.2 ± 6.0°. Buckling has also been observed in the DNA bases in the crystal structures of other perpendicular intercalator–DNA complexes. In the crystal structure of the 2:1 triostin A–[d(CGTACG)]$_2$ complex, the base pairs of the CpG buckle by about ~20° (Wang et al., 1984; Ughetto et al., 1985). The base pairs flanking the site of intercalation for both nogalamycin and daunomycin–DNA complexes curve significantly around the intercalated ring. Williams et al. (1992) have suggested that buckling is another mechanism by which the bases surrounding the site of intercalation increase their van der Waals interactions. In other words, the base pairs flanking the site of intercalation create a cavity that optimally fits the shape and position of the quinoxaline intercalator. In the case of parallel intercalators such as ethidium, buckling at the site of intercalation would be energetically unfavorable because there would be little interaction between the base and the intercalator in the middle of the long axis, while causing steric hindrance between the intercalator and the DNA bases at the ends of the long axis.

The buckling of these bases is well defined as indicated by the low RMSD for the four internal base pairs. However, in some of the structures, buckling occurs also in the terminal G·C base pairs, which raises the question of whether the buckling of the four internal base pairs is an artifact of the refinement process or whether they buckle as a result of the experimental restraints. In order to determine whether the buckling of the base pairs results from application of the experimental NOE volumes or from application of the Charmm force field, the buckling was removed from each base pair in the structure of F_1 and the R factor of the new structure was calculated. Removal of the buckling from the T_3·A_4 base pair of F_1 causes the R factor to increase from 0.208 to 0.282. The RMSD between F_1 and F_1 without the buckle of the internal base pairs is 0.08 Å. Changing the χ torsional angle of one of the T_5 bases from −116° to −100°, which removes the buckling from that A_2·T_5 base pair, causes the R factor to increase to 0.230. The RMSD between the structures with the different χ torsional angles is 0.04 Å. The structure regains its buckling when they are energy minimized in the presence of the E_{relax} pseudo energy term. Movement of one of the terminal G bases causes an increase in the R factor to 0.229. However, the RMSD between F_1 and F_1 with the displaced dG is 0.35 Å. This indicates that the R factor is more sensitive to changes in atoms in the $A_2T_3A_4T_5$ binding site than in the terminal G·C base pairs. When F_1 is energy minimized with all potential energy terms except the experimental restraints, the final structure has no buckle and the

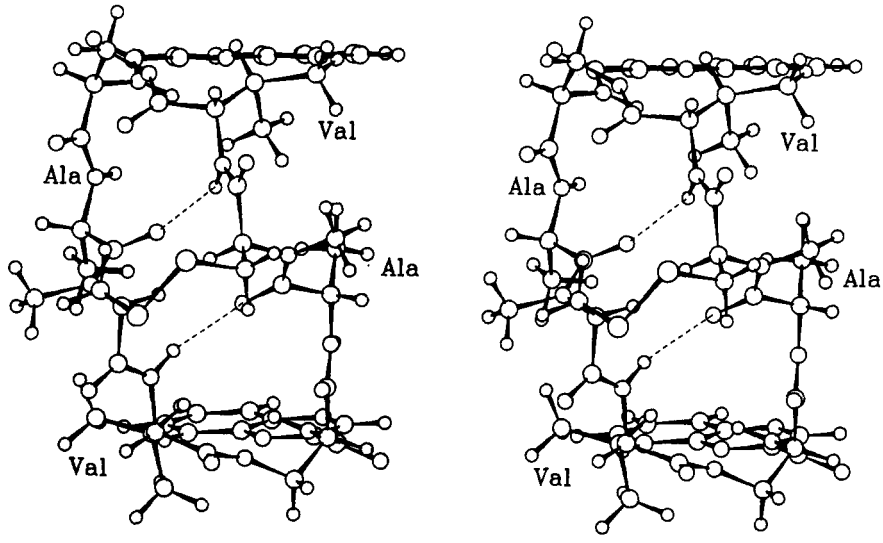

FIGURE 9: Ball and stick structure of CysMeTANDEM alone, illustrating the intramolecular hydrogen bond between the Val NH and the Ala carbonyl.

R factor increases significantly (data not shown). This indicates that the buckling occurs as a consequence of the experimental restraints.

DNA Sugar Conformation and Glycosidic Torsion Angles in the Complex. Table III lists the average values of the pseudorotation phase angle *P* for the six sugars from each strand of the DNA. All three purine sugars, G_1, A_2, and A_4, adopt C2′ endo sugar puckers. Of the pyrimidine sugars, T_5 is C1′ exo (near C2′ endo), T_3 is C4′ exo (near to C3′ endo), and C_6 is C3′ endo sugar pucker. The C3′ endo pucker displayed by C_6 appears to be an end effect, since P.COSY data from the CysMeTANDEM–d[d(GGATATCC)]$_2$ complex indicate that the C_7 sugar from the octamer exhibits a sugar pucker close to C2′ endo (Addess et al., 1992a). The C4′ exo pucker displayed by T_3 is in the N-type range observed by the C sugar of the CpG binding site of echinomycin–DNA complexes (Gao & Patel, 1988, 1989; Gilbert & Feigon, 1991, 1992) and of a 1:1 triostin A–[d(GACGTC)]$_2$ complex in solution (Addess and Feigon, unpublished results). The T_3 sugar is S-type (near C2′ endo) in the free hexamer [d(GATATC)]$_2$ (data not shown). Therefore, the T_3 sugar changes conformation to N-type as a consequence of drug binding. The conformational change of the T_3 sugar may contribute to the unwinding of the DNA at the TpA step by decreasing the distance between the 3′ and 5′ phosphates attached to T_3. In A–DNA, the helix is underwound compared to B-DNA because the average interphosphate distances along the backbone is only 5.9 Å, which is shorter than the average interphosphate distance of 7.0 Å along the backbone of B–DNA. This shorter interphosphate distance along the backbone of A–DNA is caused by the C3′ endo puckering of its deoxyribose sugars (Saenger, 1984). All of the glycosidic torsion angles are in the anti range.

Structure of CysMeTANDEM in the Complex. Figure 9 shows the stereoview of a ball and stick representation of the drug alone. There are two intramolecular hydrogen bonds, one between each Val NH and Ala CO. The average calculated distance between Val NH and the Ala CO for all 10 structures is 2.29 ± 0.10 Å. These two hydrogen bonds, which were observed in the crystal structure of TANDEM alone (Viswamitra et al., 1981; Hossain et al., 1982), cannot occur in either triostin A or echinomycin because the Val is N-methylated. Figure 10 shows views of both CysMeTANDEM and triostin A from the top. Hydrogen-bond formation

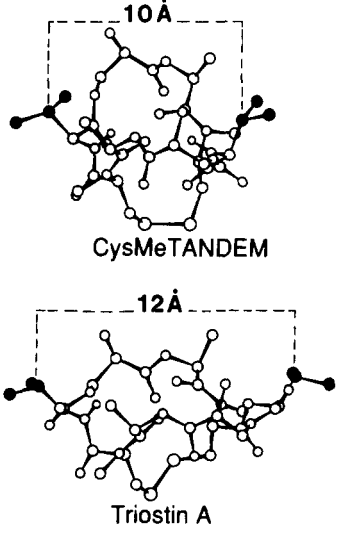

FIGURE 10: Top views of CysMeTANDEM and triostin A [from the crystal structure (Wang et al., 1986)]. Valine side chain atoms and the distance between them on both drugs are indicated.

between Val NH and Ala CO results in several differences in backbone conformation of the peptide ring of the two drugs. The distance between the Val N and the Ala CO is approximately 1 Å shorter in CysMeTANDEM than in triostin A. In triostin A there is an outward rotation of the Val Me side chains, which causes the face of the depsipeptide ring to be placed close to the floor of the minor groove (Sheldrick et al., 1984). This positions the Ala CO of triostin A close enough to form an intermolecular hydrogen bond with the exocyclic amino group of guanine of the CpG step. In the crystal structures of triostin A–DNA complexes, only one of the two possible hydrogen bonds is observed, resulting in a slightly asymmetric structure (Wang et al., 1984; Ughetto et al., 1985). However, preliminary results of a proton NMR study of triostin A complexed with the hexamer [d(GACGTC)]$_2$ indicate that the complex retains its 2-fold symmetry in solution (Addess and Feigon, unpublished results). No such hydrogen bond could form in the CysMeTANDEM–DNA complexes, regardless of the geometry of the peptide ring, since the corresponding AN2 position has an H rather than the amino group at GN2.

Table IV lists selected dihedral angles for both CysMeTANDEM in the complex presented here and triostin A in the

Table IV: Selected Dihedral Angles of the Peptide Backbone

residue	dihedral angle	triostin A (crystal)[a]	CysMeTANDEM (mean NMR)
Ser_1	N-C-CA-CB	−138	−139
	N-C-CA-N	−32	−16
	C-CA-CB-OG	64	63
Cys_1	C-CA-N-C	−139	−121
	N-C-CA-N	78	80
Ala_1	C-CA-N-C	−102	−81
	N-C-CA-N	162	157
Val_1	C-CA-N-C	−117	−129
	OG-C-CA-N	−56	−148
Ser_2	N-C-CA-CB	−177	−140
	N-C-CA-N	−51	−17
	C-CA-CB-OG	76	63
Cys_2	C-CA-N-C	−133	−124
	N-C-CA-N	73	86
Ala_2	C-CA-N-C	−63	−89
	N-C-CA-N	177	157
Val_2	C-CA-N-C	−66	−136
	OG-C-CA-N	34	−127

[a] From Wang et al. (1986).

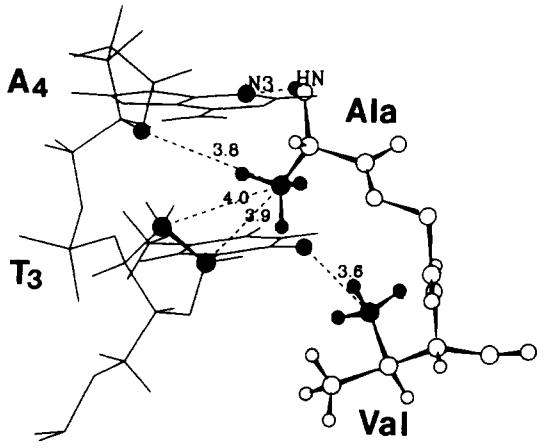

FIGURE 11: Part of the structure of the complex, showing the interactions of CysMeTANDEM at the TpA step. The two intermolecular hydrogen bonds between the AlaNH and the A_4N3 and the van der Waals interactions between the Ala methyl and the T_3C1', T_3C2', and the G_4O2' and between the Val methyl and T_3O2 are indicated.

2:1 triostin A–$[d(CGTACG)]_2$ crystal structure (Ughetto et al., 1985; Wang et al., 1986). The dihedral angles of all of the residues of the peptide ring of both drugs are similar, with the exception of the Val residues. The similarity of the dihedral angle of the D-Ser residues of both drugs is a result of intercalation. The quinoxalines are positioned perpendicular to the cyclic octadepsipeptide ring of both antibiotics as a result of the right-handed chirality of D-Ser. Furthermore, the Ala methyl and Cys N-methyl side chains have similar orientations in both antibiotics. The methyl side chains of alanine point directly into the minor groove of the DNA, while the both Cys N-methyl groups are facing perpendicular to the Ala methyls, projecting away from the minor groove. This is consistent with the evidence that the N-methyl substituents of the cysteine residues contribute little or nothing to the sequence specificity of triostin A or CysMeTANDEM (Low et al., 1986).

DNA–Drug Interactions. Intermolecular hydrogen bonds are observed between the Ala NH and the A_4N3 (Figure 11). The average calculated distance between the AlaNH and the A_4N3 from all 10 structures is 2.26 ± 0.07 Å. An equivalent hydrogen bond between GN3 and the Ala NH has been shown to exist in all complexes of the CpG specific triostin A and echinomycin (Gao & Patel, 1988; Gilbert et al., 1989; Gilbert & Feigon, 1991; Ughetto et al., 1985; Wang et al., 1984, 1986). This hydrogen bond is apparently essential for binding of CysMeTANDEM. Elimination of this hydrogen bond by substituting alanine for lactic acid causes CysMeTANDEM to lose its ability to protect Tyr I promoter DNA from DNase I, indicating that the substituted CysMeTANDEM does not bind tightly to DNA (Olsen et al., 1986).

There are several strong van der Waals interactions between CysMeTANDEM and DNA, particularly between the Ala methyl of CysMeTANDEM and the C1′ and C2′ of T_3 and the O4′ of A_4 (Figures 5 and 11). Similar interactions have been observed between the Ala methyl of triostin A and the atoms of the C sugar and G sugar of the CpG binding site (Wang et al., 1984; Ughetto et al., 1985). We also observe strong van der Waals interactions between one of the Val methyls and the O2 of thymine in the TpA step on both symmetrically related halves of the molecule (Figure 11). In the crystal structure of the 2:1 triostin A–$[d(CGTACG)]_2$ complex, the valine methyls are rotated too far outward to have strong van der Waals interactions with O2 of cytosine in the CpG step (see Figure 10).

Although the hydrogen bond between ala NH and purine N3 at the binding site is apparently essential for tight binding, it does not explain the A·T sequence specificity of CysMeTANDEM versus the C·G sequence specificity of triostin A and echinomycin. Triostin A has an additional hydrogen bond from the Ala CO to the amino group of G; if CysMeTANDEM bound to a CpG site formation of this hydrogen bond would require breaking the *intra*molecular hydrogen bond between Ala CO and the unmethylated Val NH. Lack of this hydrogen bond might decrease the binding constant of CysMeTANDEM to CpG sites but still does not explain why TpA sites are so strongly preferred. No obvious steric hindrance would be caused by the G amino group. The peptide ring of the CysMeTANDEM is narrower than triostin A due to the formation of the intramolecular hydrogen bond, and this may result in better van der Waals interactions at TpA than CpG. Another possibility is that the minor groove width at the CpG site may be wider than at the TpA site, enabling the wider peptide ring of triostin A to fit in the CpG site but not the TpA site. We examined this by superimposing the TpA site of the CysMeTANDEM complex with the CpG site in the crystal structure of the 2:1 triostin A–$[d(CGTACG)]_2$ complex (Wang et al., 1984; Ughetto et al., 1985). The RMSD for all common atoms between TpA bound by CysMeTANDEM and CpG bound by triostin A in the crystal structure of the 2:1 triostin A–$[d(CGTACG)]_2$ complex (Wang et al., 1984; Ughetto et al., 1985) is 0.55 Å (data not shown), revealing little or no difference in the minor groove width between a TpA step and a CpG step when both are bound by their respective drugs. Therefore, the minor groove of TpA is wide enough to accommodate the wider peptide ring of triostin A. Unless the minor groove width of the unbound TpA is narrower than that of the CpG and sequence specificity involves the drug's ability to recognize this difference, it appears that minor groove width has no role in the sequence specificity of these quinoxaline antibiotics. Perhaps the van der Waals interaction between Val methyl and thymine O2 may play a role in the sequence specificity of CysMeTANDEM for TpA versus CpG. We are currently determining the solution structure of a complex between triostin A and the hexamer $[d(GACGTC)]_2$ with the aim of making a direct comparison of the 1:1 triostin

A-$[d(GACGTC)]_2$ complex with the CysMeTANDEM-$[d(GATATC)]_2$ complex.

ACKNOWLEDGMENT

We thank Shiva Malek and Karl Koshlap for synthesizing and purifying the DNA and Richard K. Olsen for providing the CysMeTANDEM for these studies.

REFERENCES

Addess, K. J., Gilbert, D. E., Olsen, R. K., & Feigon, J. (1992a) *Biochemistry 31*, 339–350.

Addess, K. J., Gilbert, D. E., & Feigon, J. (1992b) in *Structure and Function Volume 1: Nucleic Acids* (Sarma, R. H., & Sarma, M. H., Eds.) pp 147–164, Adenine Press, Schenectady, NY.

Bax, A., & Davis, D. G. (1985) *J. Magn. Reson. 65*, 355–360.

Brünger, A. T. (1990) *X-PLOR (Version 2.1) Manual 1-291*, The Howard Hughes Medical Institute and Department of Molecular Biophysics and Biochemistry, Yale University, New Haven, CT.

Crippen, G., & Havel T. F. (1988) *Distance Geometry and Molecular Conformation*, Research Studies Press, Taunton, Somerset, England.

Egli, M., Williams, L. D., Frederick, C. A., & Rich, A. (1991) *Biochemistry 30*, 1364.

Feigon, J., Leupin, W., Denny, W. A., & Kearns, D. R. (1984) *J. Med. Chem. 27*, 450–465.

Gao, X., & Patel, D. J. (1988) *Biochemistry 27*, 1744–1751.

Gao, X., & Patel, D. J. (1989) *Q. Rev. Biophys. 22*, 93–138.

Gao, Y.-G., Liaw, Y.-C., Robinson, H., & Wang, A. H.-J. (1990) *Biochemistry 29*, 10307–10316.

Gilbert, D. E., & Feigon, J. (1991) *Biochemistry 30*, 2483–2494.

Gilbert, D. E., & Feigon, J. (1992) *Nucleic Acids Res. 20*, 2411–2420.

Gilbert, D. E., van der Marel, G. A., van Boom, J. H., & Feigon, J. (1989) *Proc. Natl. Acad. Sci. U.S.A. 86*, 3006–3010.

Gonzales, C., Rullman, J. A. C., Bonvin, A. M. J. J., Boelens, R., & Kaptein, R. (1991) *J. Magn. Reson. 91*, 659–664.

Haasnoot, C. A. G., De Leeuw, F. A. A. M., & Altona, C. (1980) *Tetrahedron 36*, 2783–2792.

Hossain, M. B., van der Helm, D., Olsen, R. K., Jones, P. G., Sheldrick, G. M., Egert, E., Kennard, O., Waring, M. J., & Viswamitra, M. A. (1982) *J. Am. Chem. Soc. 104*, 4301–4308.

Katagiri, K., Yoshida, T., & Sato, K. (1975) in *Antibiotics III. Mechanism of Action of Antimicrobial and Antitumour Agents* (Corcoran, J., & Hahn, F. E., Eds.), pp 234–251, Springer-Verlag, Berlin, Heidelberg, and New York.

Kim, S.-G., Lin, L.-J., & Reid, B. R. (1992) *Biochemistry 31*, 3564–3574.

Kumar, A., Ernst, R. R., & Wüthrich, K. (1980) *Biochem. Biophys. Res. Commun. 95*, 1–6.

Kuszewski, J., Nilges, M., & Brünger, A. T. (1992) *J. Biomol. NMR 2*, 33–56.

Lee, J. S., & Waring, M. J. (1978a) *Biochem. J. 173*, 115–128.

Lee, J. S., & Waring, M. J. (1978b) *Biochem. J. 173*, 129–144.

Low, C. M. L., Olsen, R. K., & Waring, M. J. (1984a) *FEBS Lett. 176*, 414–419.

Low, C. M. L., Drew, H. R., & Waring, M. J. (1984b) *Nucleic Acids Res. 12*, 4865–4879.

Low, C. M. L., Fox, K. R., Olsen, R. K., & Waring, M. J. (1986) *Nucleic Acids Res. 14*, 2015–2033.

Marion, D., & Bax, A. (1988) *J. Magn. Reson. 80*, 528–533.

Mueller, L. (1987) *J. Magn. Reson. 72*, 191–196.

Nerdal, W., Hare, D. R., & Reid, B. R., (1988) *J. Mol. Biol. 201*, 717–739.

Nilges, M., Habazettl, J., Brünger, A. T., & Holak, T. A. (1991) *J. Mol. Biol. 219*, 499–510.

Nunn, C. M., Van Meervelt, L., Zhang, S., Moore, M. H., & Kennard, O. (1991) *J. Mol. Biol. 222*, 167–177.

Olsen, R. K., Ramasamy, K., Bhat, K. L., Low, C. M. L., & Waring, M. J. (1986) *J. Am. Chem. Soc. 108*, 6032–6036.

Otting, G., Widmer, H., Wagner, G., & Wüthrich, K. (1986) *J. Magn. Reson. 66*, 187–193.

Powers, R., Olsen, R. K., & Gorenstein, D. G. (1989) *J. Biomol. Struct. Dyn. 7*, 515–553.

Saenger, W. (1984) *Principles of Nucleic Acid Structure*, Springer-Verlag, Berlin, Heidelberg, and New York.

Sheldrick, G. M., Guy, J. J., Kennard, O., Rivera, V., & Waring, M. J. (1984) *J. Chem. Soc., Perkin Trans II*, 1601–1605.

Sklenář, V., & Bax, A. (1987) *J. Magn. Reson. 75*, 378–383.

States, D. J., Haberkorn, R. A., & Ruben, D. J. (1982) *J. Magn. Reson. 48*, 286–292.

Ughetto, G., Wang, A. H.-J., Quigley, G. J., van der Marel, G. A., van Boom, J. H., & Rich, A. (1985) *Nucleic Acids Res. 13*, 2305–2323.

van Dyke, M. M., & Dervan, P. B. (1984) *Science 225*, 1122–1127.

Viswamitra, M. A., Kennard, O., Cruse, W. B. T., Egert, E., Sheldrick, G. M., Jones, P. G., Waring, M. J., Wakelin, L. P. G., & Olsen, R. K. (1981) *Nature 289*, 817–819.

Wang, A. H.-J., Ughetto, G., Quigley, G. J., Hakoshima, T., van der Marel, G. A., van Boom, J. H., & Rich, A. (1984) *Science 225*, 1115–1121.

Wang, A. H.-J., Ughetto, G., Quigley, G. J., & Rich, A. (1986) *J. Biomol. Struct. Dyn. 4*, 319–342.

Waterloh, K., Olsen, R. K., & Fox, K. R. (1992) *Biochemistry 31*, 6246–6253.

Widmer, H., & Wüthrich, K. (1987) *J. Magn. Reson. 74*, 316–336.

Williams, L. D., Egli, M., Gao, Q., & Rich, A. (1992) in *Structure and Function Volume 1: Nucleic Acids* (Sarma, R. H., & Sarma, M. H., Eds.) pp 107–125, Adenine Press, Schenectady, NY.

Yip, P., & Case, D. A. (1989) *J. Magn. Reson. 83*, 643–648.

Zhang, X., & Patel, D. J. (1990) *Biochemistry 29*, 9451–9466.